Taylor & Francis
Taylor & Francis Group

∂ OPEN ACCESS | Check for updates

Chemical fluorescence-based dye staining for 3-dimensional histopathology analysis

Hyun Jung Kim[a,b], Jeongah Kim[a], Jungyoon Choi[a] and Woong Sun[a]

[a]Department of Anatomy, College of Medicine, Korea University, Seoul, Korea; [b]Graduate School of Medical Science and Engineering, Korea Advanced Institute of Science and Technology (KAIST), Daejeon, South Korea

ABSTRACT

Tissue clearing for 3-dimensional (3D) imaging is increasingly utilized in many biomedical applications, including the pathological examination of human biopsy specimens. Although many protocols offer rapid and efficient tissue clearing (>1 d), immunofluorescence labeling of thick specimens is a highly time-consuming process. The use of low molecular weight chemical dyes has potential benefits in terms of speed and quality of 3D labeling. Accordingly, we tested several chemical dyes to assess their potential applications in 3D imaging. The combination of SYTO 16 and eosin (S&E) was found to be a potential fluorescent version of the hematoxylin–eosin (H&E) stain. Furthermore, picrosirius red (for collagen), Congo red (for senile plaques), and fluorescent Nissl (for neurons in the normal brain or blood vessels in the injured brain) stains can be used alone or in combination with antibody labeling. As chemical labeling requires a relatively short incubation time (<1 d), fluorescent chemical dyes could expedite the 3D imaging process.

Introduction

Tissue clearing methods have evolved rapidly and have been applied to image 3-dimensional (3D) structures of tissues at single-cell resolution (Ueda et al. 2020; Richardson et al. 2021). Tissue clearing can be achieved by a combination of delipidation and matching the refractive index (RI) of tissues with that of the mounting medium. Several techniques, including solution-based (several versions of CUBIC and SeeDB), organic solvent-based (versions of BABB and iDISCO), and hydrogel-based (clarity, PACT, and ACT) are available (Dodt et al. 2007; Chung et al. 2013; Ke et al. 2013; Renier et al. 2014; Susaki et al. 2014; Yang et al. 2014; Lee et al. 2016; Tainaka et al. 2018). Speed of the process, tissue deformity, and maximal clarity of the specimen vary depending on the optical properties of the tissues and the method of clearing (Gomez-Gaviro et al. 2020; Tian et al. 2021). Accordingly, many tissue-clearing methods have been customized for specific specimens (Vieites-Prado and Renier 2021). These innovations have impacted the understanding of 3D architectures of brain connectivity, embryos, and human pathological specimens (Belle et al. 2017; Nojima et al. 2017; Winnubst et al. 2019).

The application of these innovative tissue clearing tools for histopathological analysis requires several modifications to meet the criteria that are followed in routine histopathology labs. For instance, the duration of the labeling process should be short, preferably within 5 working days. Many tissue-clearing methods offer relatively rapid clearing. In particular, specimens with low lipid content can be cleared faster as RI-matching is sufficient for clearing. However, the delipidation step cannot be eliminated in many specimens, and the inclusion of the delipidation step considerably increases the total duration of the process. The use of electrical fields for active delipidation significantly shortens the duration of tissue-clearing processes, and whole mouse brain clearing can be achieved within one day (Chung et al. 2013; Kim et al. 2015; Lee et al. 2016).

Another factor that significantly contributes to processing time is labeling. Most tissue-clearing methods are optimized for the detection of endogenous fluorescence or fluorescence signals from antibody reactions (Murray et al. 2015; Park et al. 2018; Cai et al. 2019; Zhao et al. 2020). Unfortunately, the diagnostic use of endogenous fluorescence signals from human specimens is limited, and antibody labeling of thick specimens is challenging owing to the long incubation time, uneven labeling, and clogging of the antibodies on the surface (Lai et al. 2018; Zhao et al. 2020). These

limitations are mainly caused by the slow diffusion of large molecular weight antibodies. As a result, the use of low molecular weight fluorescent chemicals that preferentially label some components within tissues has garnered remarkable attention. For instance, nuclear staining with SYTO 16, blood vessel labeling with the lipophilic dye Dil, and amyloid plaque labeling with Congo red have been successfully used for tissue 3D imaging (Liebmann et al. 2016; Lai et al. 2017).

As normal histopathological tests often involve general staining such as hematoxylin–eosin (H&E) staining (No et al. 2021; Roh et al. 2021), the development of a fluorescence staining equivalent to H&E staining is important. Eosin labels cytosol in red and exhibits red fluorescence via the conventional rhodamine filter setup of a fluorescence microscope. Thus, we determined whether eosin can be used for fluorescence counterstaining of cytosol. Combined with nuclear fluorescent dyes, such as SYTO 16, a fluorescent version of H&E staining (S&E staining), could be established, which can be an alternative to colorimetric H&E staining. We also tested whether other chemical dyes could be used for the fluorescence labeling of thick specimens.

Materials and methods

Specimens

Mouse organs were obtained from 8–10 week-old C57BL/6J mice (Koatech, Pyeong-taek, Korea). For the acute kidney injury model, 8-week-old mice were administered folic acid (Sigma #F8758) dissolved in 300 mM NaHCO$_3$ via intraperitoneal injection at a dose of 250 mg/kg. The vehicle was injected as a control, and bilateral kidneys were harvested 7 days after the injection. Cryogenic traumatic brain injury (cTBI) was induced by placing a metal probe (5 mm diameter) cooled in liquid nitrogen on the cranium of mice for 30 s (Kim et al. 2016), and the damaged brains were harvested 7 days after injury. All animal handling protocols were approved by members of the Korea University

Institutional Animal Care and Use Committee (KUIACUC-20150520-1 and KOREA-2019-0014). Human tissues were obtained from cadaver donors at the Department of Anatomy, Korea University, through the Korea University Anatomical Donation Program and treated by the university guidelines. The cadavers were fixed with 10% formalin by perfusion and kept at 4 °C for more than 2 years.

Tissue clearing

For tissue clearing, we used the ACT-PRESTO protocol reported in our previous study (Lee et al. 2016). Briefly, fixed samples were washed with PBS and incubated with polymerization buffer (A4B0; 4% acrylamide in 0.1× PBS supplemented with 0.25% photoinitiator 2,2′-azobis[2-(2-imidazolin-2-yl)propane] dihydrochloride; Wako Pure Chemical, Osaka, Japan) overnight at 4 °C. The embedded samples were polymerized for 2 h at 37 °C and −70 kPa in the X-CLARITY^{TM} Polymerization System (Logos Biosystems, Anyang, Korea). After excessive washing, the samples were placed in a tissue container in an electrophoretic tissue clearing (ETC) chamber and processed at 1.5 mA and 37 °C. Depending on the type of tissue, the ETC time varies from 3 to 24 h. The cleaned samples were washed with PBS overnight at room temperature with shaking before staining.

Staining of the specimens

Cleared samples were immersed in eosin solution at 37 °C overnight. For the S&E staining, SYTO 16 (Invitrogen #S7578, 1:500) solution was co-incubated with the eosin solution. The stained samples were washed three times with PBS for 30 min and immersed in CUBIC-mount (CM) solution for 1 h before imaging [4]. Fluorescent Nissl, Conge red, or picrosirius red were co-stained with secondary antibodies, followed by PBS washing. For picrosirius red staining, the stained samples were washed twice with acetic acid and immersed in CM solution for 1 h before imaging. The details of the fluorescence staining solutions are present in Table 1. For additional antibody staining, Na$^+$/K$^+$ATPase (Sigma #A276, 1:500), β-amyloid (Millipore #AB5078P, 1:500), E-cadherin (Cell Signaling # 3195, 1:50), type 1 collagen (Abcam #ab34710, 1:500), NeuN (Millipore #MAB377, 1:500), and GFAP (Invitrogen #13-0300, 1:500) were used prior to chemical staining.

Imaging and image processing

Cleared tissues immersed in the CM solution were used for 3D imaging. Gross images were captured using a

Table 1. Fluorescence dyes used in the study

Fluorescent Probes	Stained Tissues	Dilution	Excitation/ Emission (nm)	Supplier
Eosin Y	Eosinophilic tissues or cells	1:500	510/535	Sigma #230251
Picrosirius red	Connective tissue	1:10	561/635-685	Abcam #ab150681
Nissl	Neuron	1:250	530/615	ThermoFisher #N21482
Congo red	Amyloid	1:500	497/614	Sigma #C6277

digital camera (Canon, Tokyo, Japan) at different time points during the ETC. 3D images were acquired using a TCS SP8 confocal laser scanning microscope (Leica, Wetzlar, Germany) with a 10x lens (N.D. 0.4; W.D. 2.2 mm), 25x lens (N.D. 0.95; W.D. 2.4 mm), and 63x lens (N.D.; W.D.). Z-stack images were converted into 3D images using the Leica LAS X program, and projection images were processed using Adobe Photoshop CS6. To calculate the signal-to-noise ratio for each image, the intensity profiles of a single image were obtained using ImageJ software.

Results

Assessment of eosin as a fluorescent dye for ACT-processed organs

As test specimens, we obtained human livers and kidneys ($2 \times 2 \times 0.4$ cm) from donated cadavers. The entire process for ACT-based tissue clearing, which included fixation (overnight), acrylamide monomer infusion (overnight), polymerization, and ETC, was conducted in 3 days (Figure 1A). For sufficient clearing (>70% transparency), 6–12 h of ETC and immersion of the specimen in RT-matching CM solution were necessary (Figure 1B). After the 6-hour ETC, the samples were washed with PBS, immersed into different concentrations of eosin solution overnight, and de-stained overnight (Figure 1C). Fluorescence signals of eosin were readily detectable throughout the tissue slices (depth-wise), and the initial concentration of eosin (0.1-2%) did not significantly affect the final fluorescence intensity and evenness of the labeling in the z-axis, presumably owing to sufficient de-staining. These results suggest that a wide range of eosin concentrations can be used for efficient 3D imaging. Eosin staining can be combined with the green nuclear counterstaining dye, SYTO 16, which is widely used for 3D imaging (Tainaka et al. 2014; Lee et al. 2016). Accordingly, single cell-resolution 3D structures of mouse tissues, including the lung, liver, kidney, and colon, were visualized by S&E co-staining in a 2-day procedure (Figure 1D), allowing the entire procedure to be performed within one week.

Combination of chemical fluorescence labeling with specific immunofluorescence staining

As general colorimetric staining is often combined with specific antibody staining for precise diagnostics, we determined whether S&E staining could be combined with immunofluorescence labeling. Briefly, we incubated ETC-processed specimens with primary antibodies overnight. Thereafter, the specimens were washed, and then incubated with a mixed solution of secondary antibodies and S&E overnight (Figure 2A). Using this approach, multi-color combinatorial labeling of specific protein epitopes (Na-K-ATPase) and S&E was successfully achieved in kidney specimens (Figure 2B). Similarly, other combinations of fluorescent chemical reactions with antibody staining were tested. For instance, fluorescent Nissl staining can be used for neuronal staining of the brain (Figure 2C). Congo red staining, which can label senile plaques, was also combined with antibody staining of beta-amyloid in human brain specimens (Figure 2D). In addition, picrosirius red, which stains the extracellular matrix, can be co-labeled with E-cadherin in the kidney (Figure 2E).

Imaging of histopathology in animal models

To establish an experimental model of nephropathy, mice were administered folic acid (FA) for 7 days. FA treatments are known to promote kidney fibrosis (Yuan et al. 2003). Clearing of the FA-treated kidneys revealed atrophy of the kidneys with focal damage (Figure 3A). These pathological features were recognized via chemical imaging of the ECM deposits by picrosirius red staining, which was similar to the immunofluorescence staining of collagen type 1 (Figure 3A). Brain trauma could also be mapped using fluorescent Nissl staining (Figure 3B). Interestingly, labeled cells in the brain trauma samples were primarily blood vessels, as reported previously (Damisah et al. 2017). In combination with Nissl and GFAP antibody staining, a close association between astrogliosis and tissue remodeling with vasculature changes was readily visualized in 3D (Figure 3C).

Discussion

In this study, we demonstrated that the combination of SYTO 16 and eosin (S&E) can be used as a fluorescent version of the H&E stain. As S&E staining can be performed within one day, the total duration of specimen labeling from harvest, fixation, clearing, labeling, and imaging was less than one week. Therefore, this protocol can be used in histopathological tests during routine clinical examinations. Furthermore, by including these fluorescent dyes into the secondary antibody reaction solution, chemical staining can be combined with antibody reaction, and the duration of the protocol gets extended by only 1–2 days, which increases the feasibility of the protocol. The feasibility of the protocol was also verified using two experimental pathology
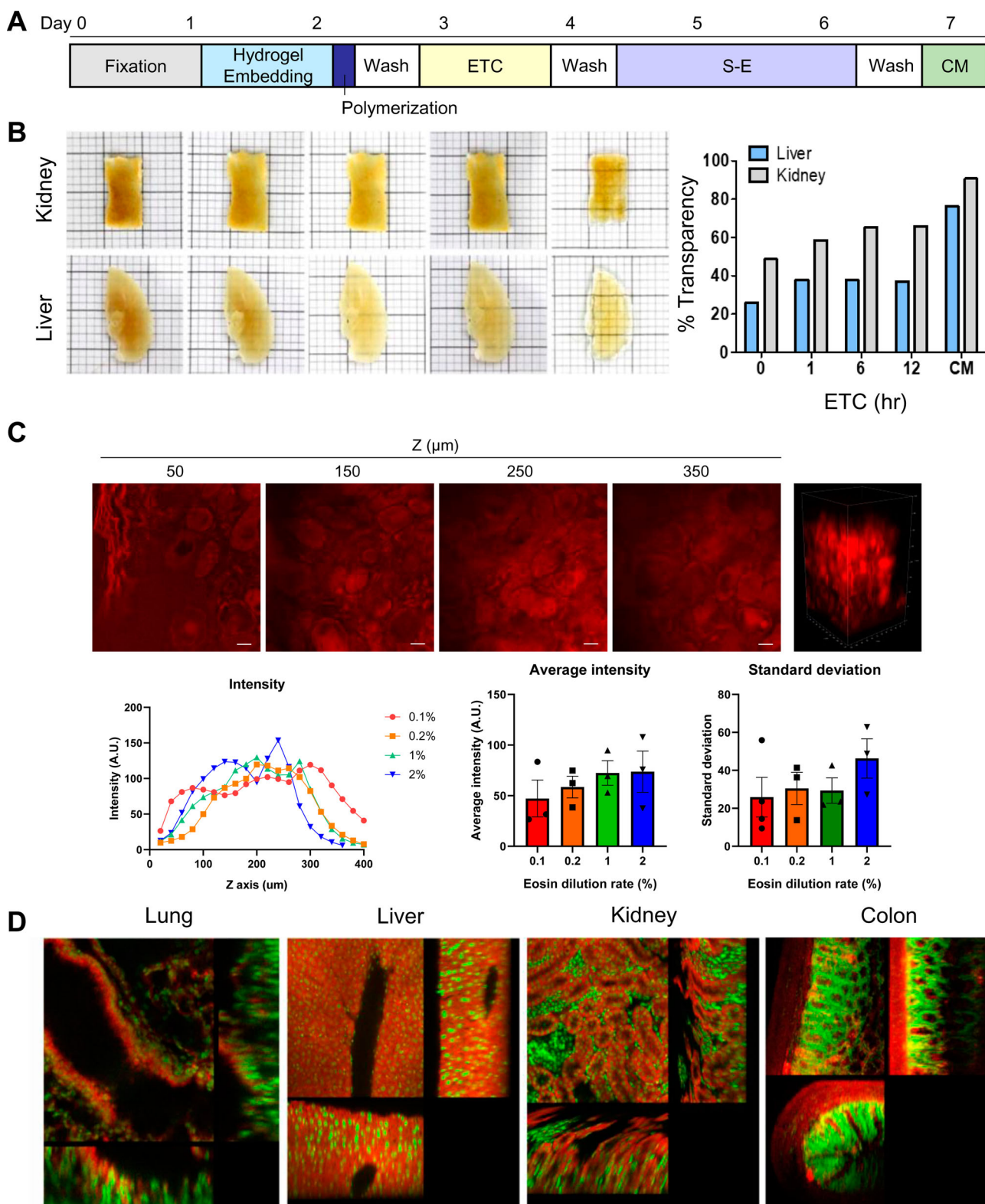
Figure 1. SYTO 16-eosin staining for 3D tissue imaging (A) Experimental scheme for tissue clearing and staining. (B) Images of human kidney (upper) and liver (lower) during electrophoretic tissue clearing (ETC). Tissue samples were placed on graph paper with a 1-mm grid. Bar graph showing the transparency rate of the specimens at 0, 1, 6, 12 h of ETC, in CUBIC-mount solution. (C) Eosin staining of 1 mm-thick human kidney specimens was imaged at different depths and converted into 3D images (upper). Scale = 20 μm. The mean intensity at different depths, average intensity, and standard deviation of mean intensity was measured from the Z-stack images with different eosin dilutions (lower). Mean ± S.E.M (D) SYTO 16-eosin staining of multiple mouse organs. Z-projections in the X-Z direction (lower) and the Y-Z direction (right) are shown in every optical slice. Scale = 100 μm.
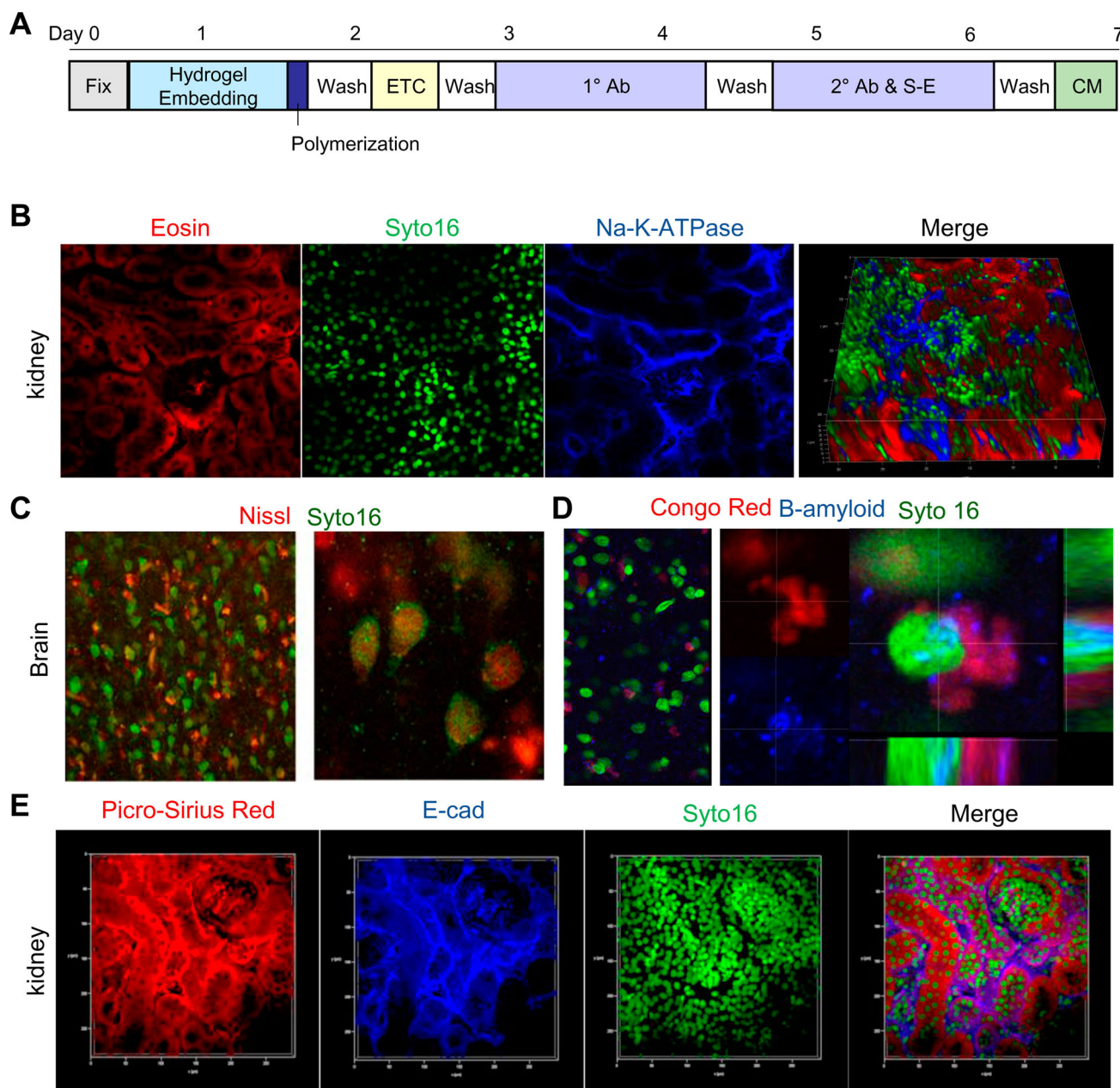
Figure 2. Use of various chemical fluorescent dyes for 3D tissue imaging (A) Experimental scheme for tissue clearing and staining. (B) SYTO 16-eosin staining of 1 mm-thick mouse kidney specimens in combination with NA-K-ATPase antibody staining. Single-plane images with different color channels were obtained from Z-stack images and converted into 3D images (right). (C) Single-plane images of 1 mm-thick human brain specimens with SYTO 16 and Nissl staining. Scale = 50 μm. (D) A single-plane image of 1 mm-thick human brain specimen with SYTO 16, Congo red, and β-amyloid staining (left). Scale = 50 μm. High magnification Z-stacked images of a single cell with senile plaques, indicated with z-projections in the X-Z direction (lower) and the Y-Z direction (right). Scale = 10 μm. (E) SYTO 16-eosin staining of 1 mm-thick mouse kidney specimens with picrosirius red staining. 3D images were separated by color channels.

models. Based on our findings, pathological symptoms in the experimental models were readily detectable by fluorescence imaging.

Other fluorescent dyes, such as Congo red, fluorescent Nissl, and picrosirius red, are compatible with the ACT-based tissue clearing protocol, and are used to label senile plaques, neurons, and ECM in the tissue, respectively. Although chemical dyes can be readily utilized in a laboratory setting, there are some limitations. Since chemical dyes stain biological macromolecules less specifically, they may exhibit a reduced contrast compared with antibody staining, and the target tissue components may change depending on the tissue status, as seen in Nissl staining of brain trauma sample.
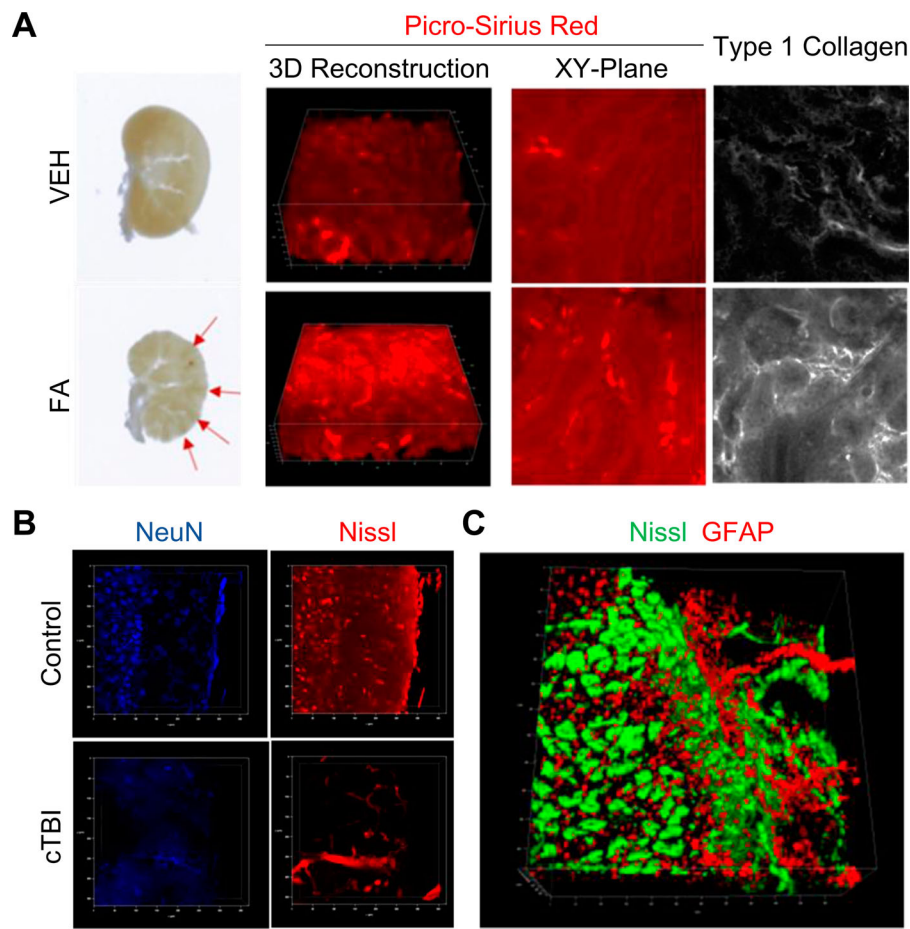
Figure 3. Chemical fluorescent dyes for histopathological analysis in 3D (A) Representative images of vehicle or folic acid (FA)-treated kidneys (left). Red arrows indicate dense fibrotic areas. Scale = 5 mm. Picrosirius red and type I collagen staining was used to detecting fibrotic changes in the FA-treated kidney tissue (right). Scale = 50 μm. (B) 3D images of Nissl staining in a cryogenic traumatic brain injury (cTBI) model. Fluorescent Nissl and NeuN labeled neurons and/or microvessels in the injured brain. Scale = 100 μm. (C) A 3D image of Nissl and GFAP staining in cTBI brain. Scale = 100 μm.

Thus, researchers must optimize/validate the staining procedure for each tissue specimen. Accordingly, our current studies emphasize the advantages of small molecular weight dyes and chemical fluorescence dyes for 3D tissue imaging. The identification of other chemicals that can detect specific tissue components will thus expedite the wide use of these techniques for 3D imaging.

Disclosure statement

No potential conflict of interest was reported by the author(s).

Funding

References

Belle M, Godefroy D, Couly G, Malone SA, Collier F, Giacobini P, Chedotal A. 2017. Tridimensional visualization and analysis of early human development. Cell. 169(1):161–173. e12 e112.

Cai R, Pan C, Ghasemigharagoz A, Todorov MI, Forstera B, Zhao S, Bhatia HS, Parra-Damas A, Mrowka L, Theodorou D et al. 2019. Panoptic imaging of transparent mice reveals whole-body neuronal projections and skull-meninges connections. *Nat Neurosci*. 22(2):317-327.

Chung K, Wallace J, Kim SY, Kalyanasundaram S, Andalman AS, Davidson TJ, Mirzabekov JJ, Zalocusky KA, Mattis J, Denisin AK, et al. 2013. Structural and molecular interrogation of intact biological systems. Nature. 497(7449):332–337.

Damisah EC, Hill RA, Tong L, Murray KN, Grutzendler J. 2017. A fluoro-Nissl dye identifies pericytes as distinct vascular mural cells during in vivo brain imaging. Nat Neurosci. 20 (7):1023–1032.

Dodt HU, Leischner U, Schierloh A, Jahrling N, Mauch CP, Deininger K, Deussing JM, Eder M, Zieglgansberger W, Becker K. 2007. Ultramicroscopy: three-dimensional visualization of neuronal networks in the whole mouse brain. Nat Methods. 4(4):331–336.

Gomez-Gaviro MV, Sanderson D, Ripoll J, Desco M. 2020. Biomedical applications of tissue clearing and three-dimensional imaging in health and disease. iScience. 23(8):101432.

Ke MT, Fujimoto S, Imai T. 2013. Seedb: a simple and morphology-preserving optical clearing agent for neuronal circuit reconstruction. Nat Neurosci. 16(8):1154–1161.

Kim JY, Choi K, Shaker MR, Lee JH, Lee B, Lee E, Park JY, Lim MS, Park CH, Shin KS, et al. 2016. Promotion of cortical neurogenesis from the neural stem cells in the adult mouse subcallosal zone. Stem Cells. 34(4):888–901.

Kim SY, Cho JH, Murray E, Bakh N, Choi H, Ohn K, Ruelas L, Hubbert A, McCue M, Vassallo SL et al. 2015. Stochastic electrotransport selectively enhances the transport of highly electromobile molecules. *Proc Natl Acad Sci U S A.* 112(46): E6274-E6283.

Lai HM, Liu AKL, Ng HHM, Goldfinger MH, Chau TW, DeFelice J, Tilley BS, Wong WM, Wu W, Gentleman SM. 2018. Next generation histology methods for three-dimensional imaging of fresh and archival human brain tissues. Nat Commun. 9 (1):1066.

Lai HM, Ng WL, Gentleman SM, Wu W. 2017. Chemical probes for visualizing intact animal and human brain tissue. Cell Chem Biol. 24(6):659–672.

Lee E, Choi J, Jo Y, Kim JY, Jang YJ, Lee HM, Kim SY, Lee HJ, Cho K, Jung N, et al. 2016. ACT-PRESTO: rapid and consistent tissue clearing and labeling method for 3-dimensional (3D) imaging. Sci Rep. 6:18631.

Liebmann T, Renier N, Bettayeb K, Greengard P, Tessier-Lavigne M, Flajolet M. 2016. Three-dimensional study of Alzheimer's disease hallmarks using the iDISCO clearing method. Cell Rep. 16(4):1138–1152.

Murray E, Cho JH, Goodwin D, Ku T, Swaney J, Kim SY, Choi H, Park YG, Park JY, Hubbert A, et al. 2015. Simple, scalable proteomic imaging for high-dimensional profiling of intact systems. Cell. 163(6):1500–1514.

No H, Nam SH, Seo HW, Seo J, Park SH, Kim SB, Jung JS, Park J, Choi J, Lee JY, et al. 2021. Purple corn extract alleviates 2,4-dinitrochlorobenzene-induced atopic dermatitis-like phenotypes in BALB/c mice. Animal Cells Syst (Seoul). 25(5):272–282.

Nojima S, Susaki EA, Yoshida K, Takemoto H, Tsujimura N, Iijima S, Takachi K, Nakahara Y, Tahara S, Ohshima K, et al. 2017. Cubic pathology: three-dimensional imaging for pathological diagnosis. Sci Rep. 7(1):9269.

Park YG, Sohn CH, Chen R, McCue M, Yun DH, Drummond GT, Ku T, Evans NB, Oak HC, Trieu W, et al. 2018. Protection of tissue physicochemical properties using polyfunctional crosslinkers. Nat Biotechnol. 37:78–83.

Renier N, Wu Z, Simon DJ, Yang J, Ariel P, Tessier-Lavigne M. 2014. Idisco: a simple, rapid method to immunolabel large tissue samples for volume imaging. Cell. 159(4):896–910.

Richardson DS, Guan W, Matsumoto K, Pan C, Chung K, Erturk A, Ueda HR, Lichtman JW. 2021. Tissue clearing. Nature Reviews Methods Primers. 1(1):84.

Roh JS, Jeong H, Lee B, Song BW, Han SJ, Sohn DH, Lee SG. 2021. Mirodenafil ameliorates skin fibrosis in bleomycin-induced mouse model of systemic sclerosis. Animal Cells and Systems). 25(6):387–395.

Susaki EA, Tainaka K, Perrin D, Kishino F, Tawara T, Watanabe TM, Yokoyama C, Onoe H, Eguchi M, Yamaguchi S, et al. 2014. Whole-brain imaging with single-cell resolution using chemical cocktails and computational analysis. Cell. 157(3):726–739.

Tainaka K, Kubota SI, Suyama TQ, Susaki EA, Perrin D, Ukai-Tadenuma M, Ukai H, Ueda HR. 2014. Whole-body imaging with single-cell resolution by tissue decolorization. Cell. 159(4):911–924.

Tainaka K, Murakami TC, Susaki EA, Shimizu C, Saito R, Takahashi K, Hayashi-Takagi A, Sekiya H, Arima Y, Nojima S, et al. 2018. Chemical landscape for tissue clearing based on hydrophilic reagents. Cell Rep. 24(8):2196–2210.e9. e2199.

Tian T, Yang Z, Li X. 2021. Tissue clearing technique: recent progress and biomedical applications. J Anat. 238(2):489–507.

Ueda HR, Erturk A, Chung K, Gradinaru V, Chedotal A, Tomancak P, Keller PJ. 2020. Tissue clearing and its applications in neuroscience. Nat Rev Neurosci. 21(2):61–79.

Vieites-Prado A, Renier N. 2021. Tissue clearing and 3D imaging in developmental biology. Development. 148(18.

Winnubst J, Bas E, Ferreira TA, Wu Z, Economo MN, Edson P, Arthur BJ, Bruns C, Rokicki K, Schauder D, et al. 2019. Reconstruction of 1,000 projection neurons reveals New cell types and organization of long-range connectivity in the mouse brain. Cell. 179(1):268–281.e13. e213.

Yang B, Treweek JB, Kulkarni RP, Deverman BE, Chen CK, Lubeck E, Shah S, Cai L, Gradinaru V. 2014. Single-cell phenotyping within transparent intact tissue through whole-body clearing. Cell. 158(4):945–958.

Yuan HT, Li XZ, Pitera JE, Long DA, Woolf AS. 2003. Peritubular capillary loss after mouse acute nephrotoxicity correlates with down-regulation of vascular endothelial growth factor-A and hypoxia-inducible factor-1α. Am J Pathol. 163 (6):2289–2301.

Zhao S, Todorov MI, Cai R, Maskari RA, Steinke H, Kemter E, Mai H, Rong Z, Warmer M, Stanic K, et al. 2020. Cellular and molecular probing of intact human organs. Cell. 180(4):796–812..e19 e719.